Supporting Information

Highly reversible Zn electrodeposition enabled by glutathione-protected copper nanoclusters for aqueous Zn-ion batteries

Lu-Fan Wang, Xiao-Yuan Wang, Shu Xu, Zhou Wu, Guoqiang Sun*, Xiao-Fei Liu*, Ren-Wu Huang and Shuang-Quan Zang

Henan Key Laboratory of Crystalline Molecular Functional Materials, Green Catalysis Center, College of Chemistry, Zhengzhou University, Zhengzhou 450001, Henan, China.

*Corresponding authors.
E-mail address: sungq@zzu.edu.cn; liuxiaofei@zzu.edu.cn

Calculations:

The depth of discharge (DOD) of the Zn anode is calculated as follows:[1]

$$\mathrm{DOD}=\frac{y}{C_{Zn,volume}\cdot x\times 10^{-4}}\times 100\%=\frac{y}{0.585x}\times 100\% \quad (1)$$

Where x (μm) represents the thickness of the zinc foil used, y (mAh cm^{-2}) is areal capacity, and $C_{Zn,volume}$ (5854 mAh cm^{-3}) represents theoretical volume capacity.

$$\mathrm{DOD}=\frac{y}{C_{Zn,mass}\cdot m\times 10^{-3}}\times 100\%=\frac{y}{x}\times 100\% \quad (2)$$

Where x (mAh cm^{-2}) represents pre-deposited Zn areal capacity, y (mAh cm^{-2}) represents the actual areal capacity used during the testing, $C_{Zn,mass}$ (820 mAh g^{-1}) is theoretical mass capacity, and m (mg cm^{-2}) represents pre-deposited Zn mass.

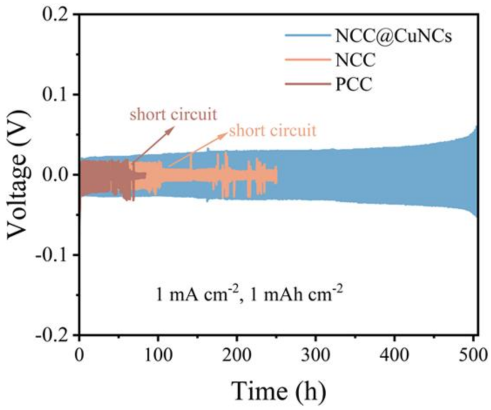

Fig. S1 Galvanostatic cycling of symmetric cells of Zn//NCC@CuNCs, Zn//NCC, and Zn//PCC at 1 mA cm^{-2}, 1 mAh cm^{-2}.

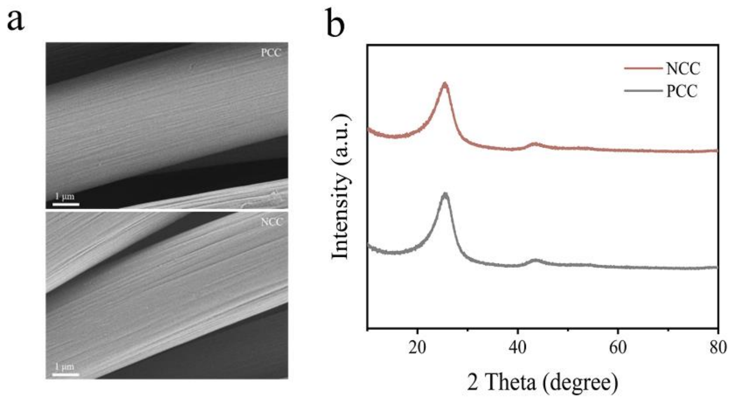

Fig. S2 (a) SEM images (b) XRD profiles of PCC and NCC.

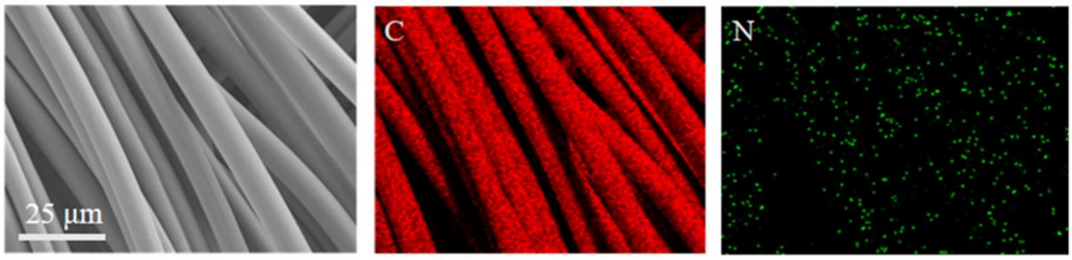

Fig. S3 SEM image of NCC and distribution of C, N elements.

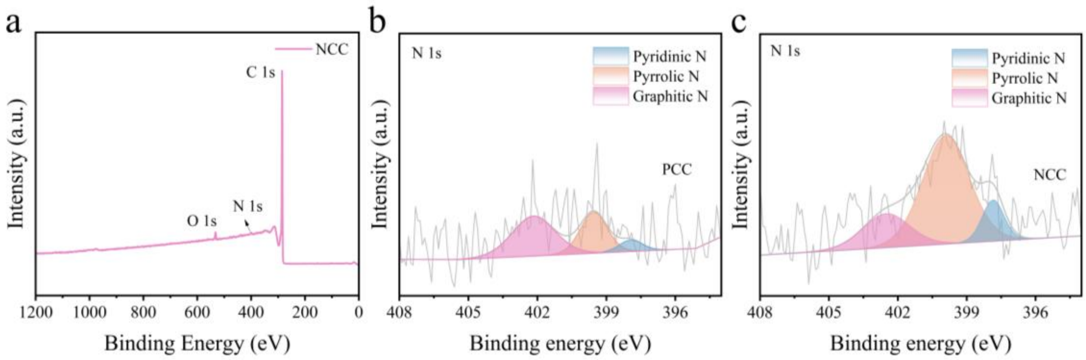

Fig. S4 (a) XPS survey spectrum of NCC. XPS high-resolution N 1s spectra of (b) PCC and (c) NCC.

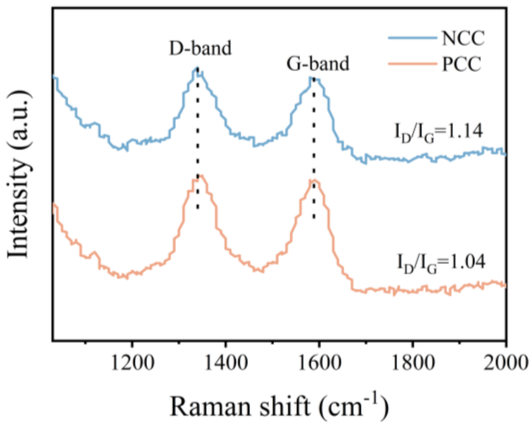

Fig. S5 Raman spectra of PCC and NCC samples.

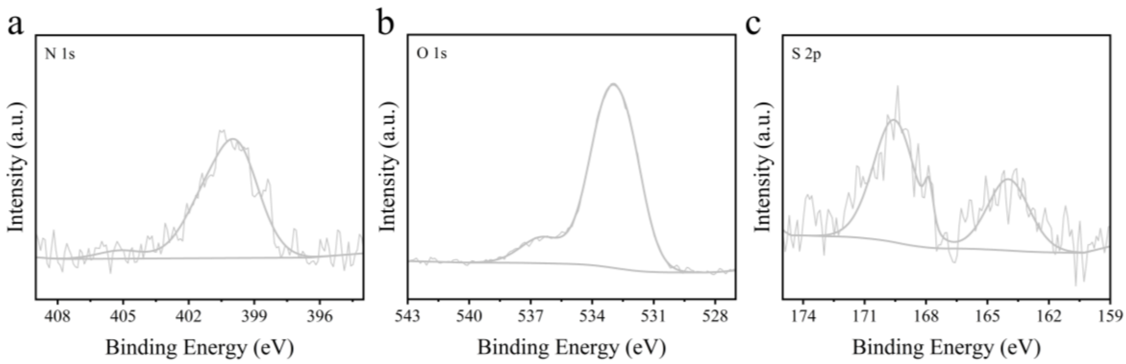

Fig. S6 XPS high-resolution spectra of NCC@CuNCs: (a) N 1s, (b) O 1s, (c) S 2p.

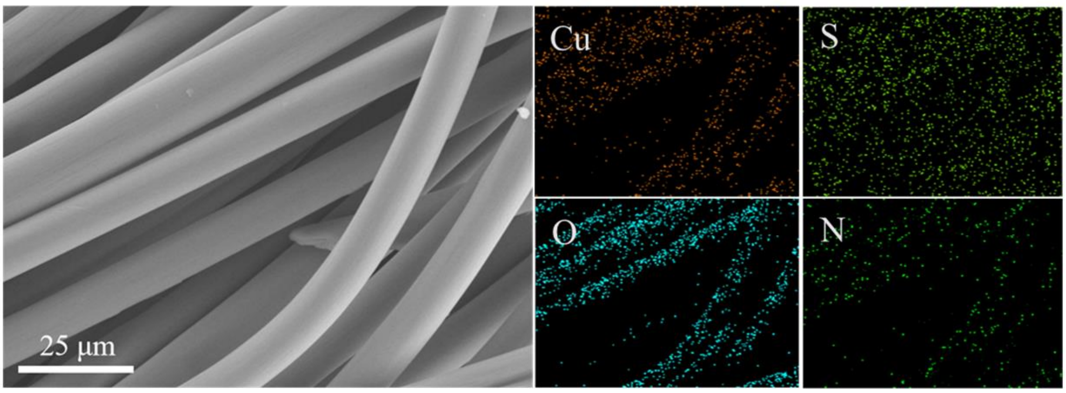

Fig. S7 SEM image of NCC@CuNCs with EDS mappings of Cu, S, O, and N elements, respectively.

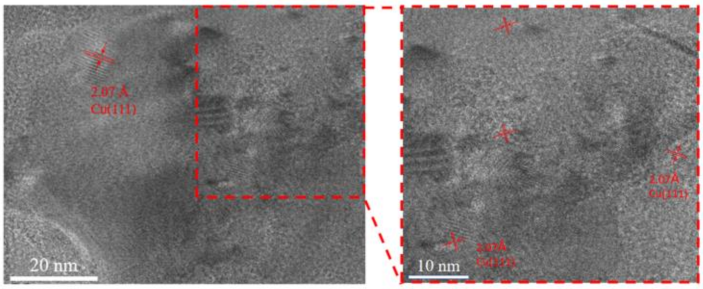

Fig. S8 TEM image and partial magnification of NCC@CuNCs.

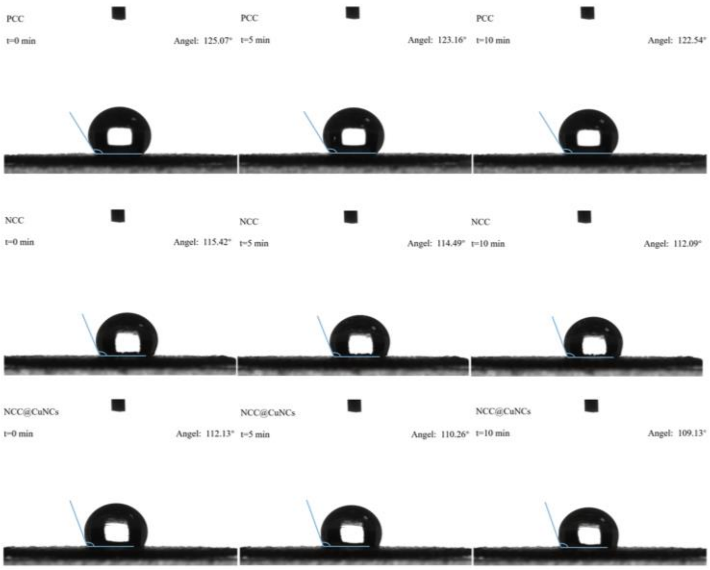

Fig. S9 Contact angle measurements of the 2 M $ZnSO_4$ electrolyte on PCC, NCC, and NCC@CuNCs substrates in the initial state and at rest for 5 and 10 minutes, respectively.

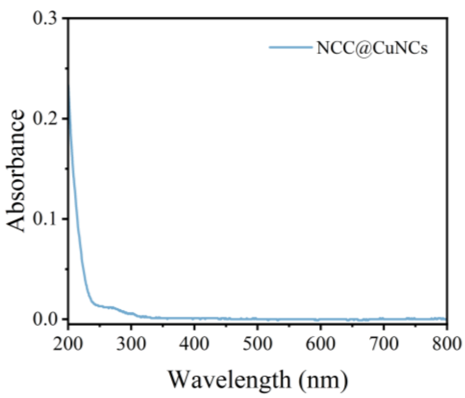

Fig. S10 UV-vis image of NCC@CuNCs substrate after Zn deposition/stripping of equal capacity (5 mAh cm^{-2}).

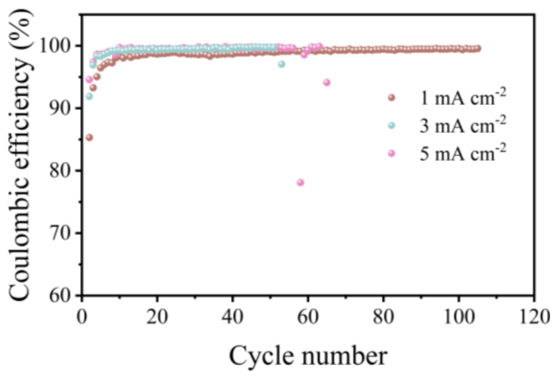

Fig. S11 Asymmetric batteries test of Zn//PCC@CuNCs at current densities of 1, 3, and 5 mA cm^{-2} respectively.

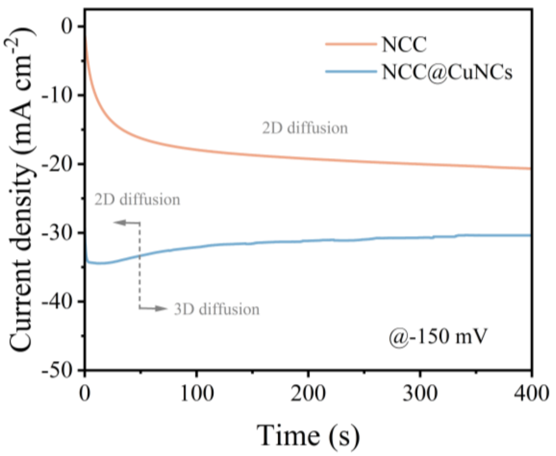

Fig. S12 Chronoamperometry curves of NCC and NCC@CuNCs at a constant voltage of -150 mV.

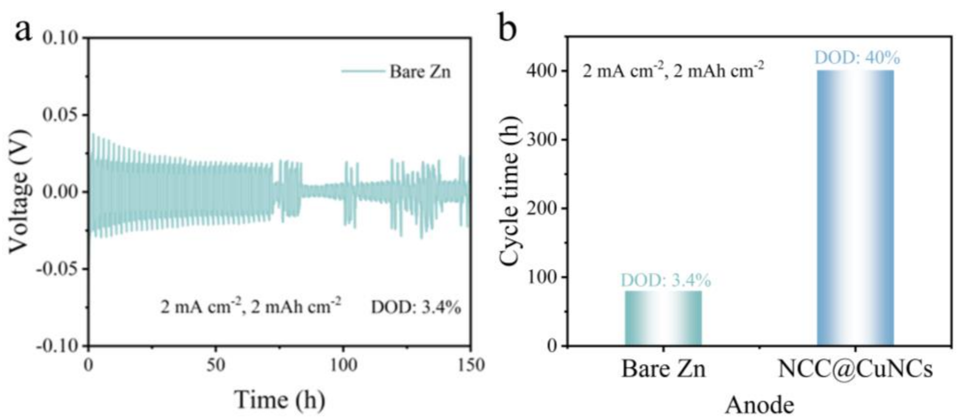

Fig. S13 (a) Galvanostatic cycling of symmetric cell of Zn//Zn at 2 mA cm^{-2}. (b) Cycling performance of symmetric cells Zn//Zn and Zn//NCC@CuNCs at 2 mA cm^{-2}.

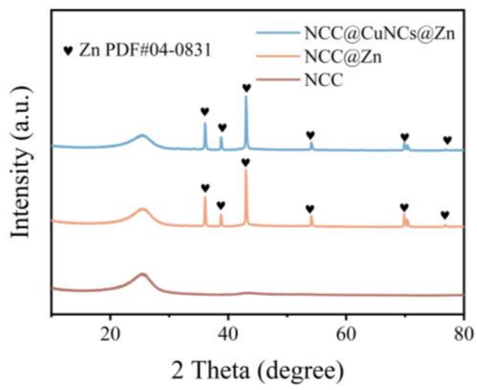

Fig. S14 XRD patterns of NCC, NCC@Zn and NCC@CuNCs@Zn.

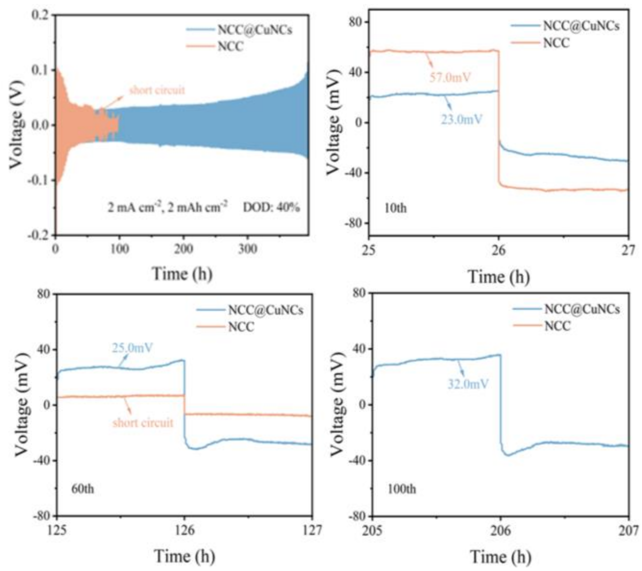

Fig. S15 Galvanostatic cycling of symmetric cells of Zn//NCC, Zn//NCC@CuNCs at 2 mA cm^{-2}, 2 mAh cm^{-2} (attached pictures: Enlarged diagrams of voltage profiles of Zn//NCC and Zn//NCC@CuNCs at the 10, 60 and 100 cycles).

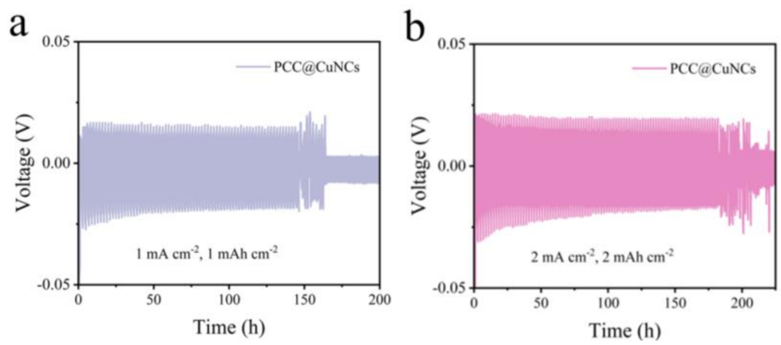

Fig. S16 Galvanostatic cycling of symmetric cells of Zn//PCC@CuNCs at (a) 1 mA cm^{-2}, 1 mAh cm^{-2} and (b) 2 mA cm^{-2}, 2 mAh cm^{-2}.

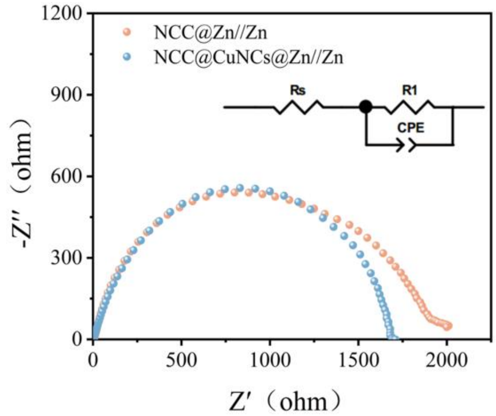

Fig. S17 Impedance diagrams of symmetric cells NCC@Zn//Zn and NCC@CuNCs@Zn//Zn.

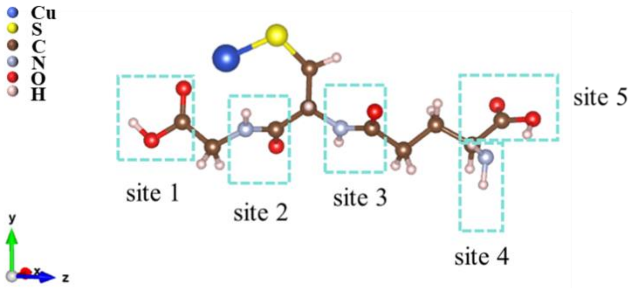

Fig. S18 Molecular model of single GSH ligand on CuNCs for computation.

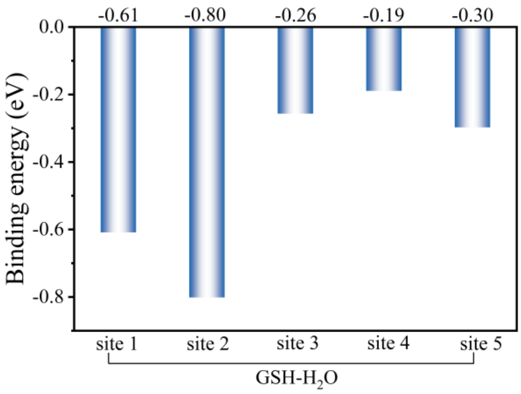

Fig. S19 The hydrogen bonding force of glutathione with water at different active sites.

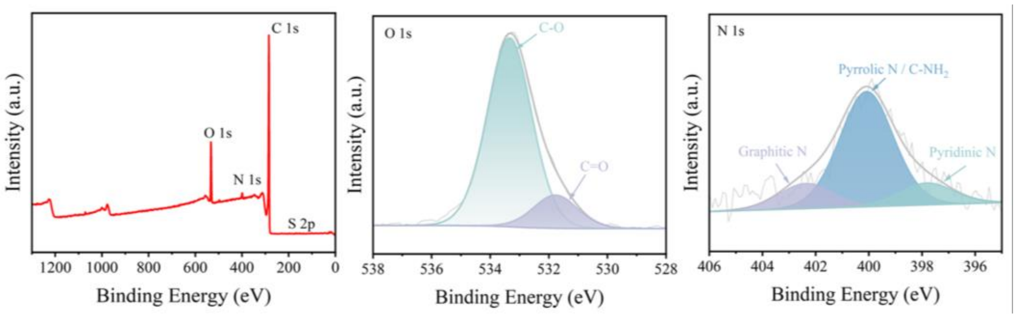

Fig. S20 XPS spectra of NCC@GSH.

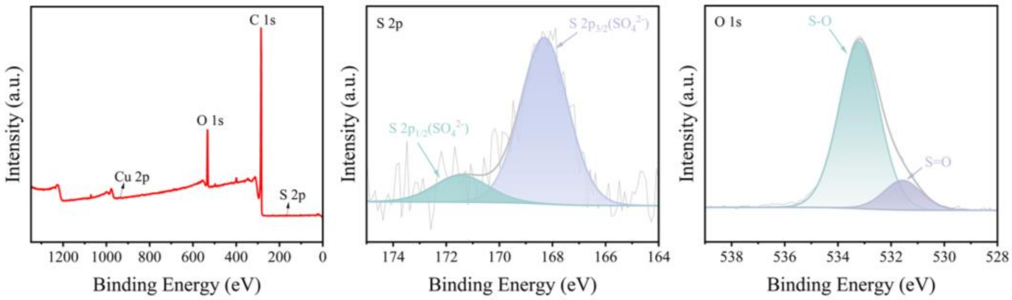

Fig. S21 XPS spectra of NCC@$CuSO_4$.

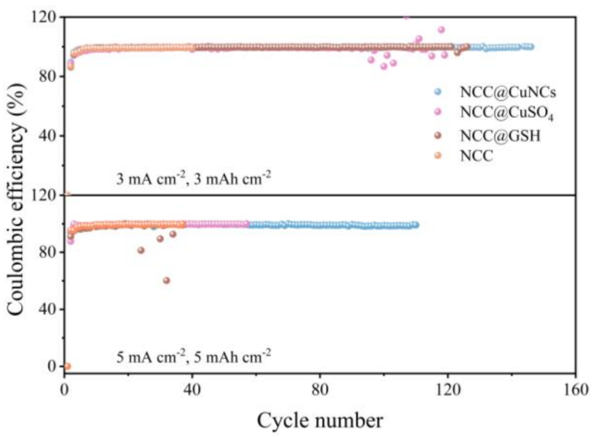

Fig. S22 CE comparison diagrams of four different kinds of asymmetric cells based on different current collectors at current densities of 3 mA cm^{-2} and 5 mA cm^{-2}.

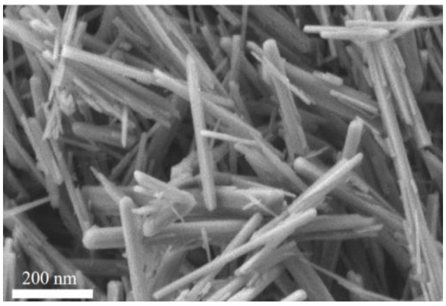

Fig. S23 SEM image of β-MnO_2 cathode material.

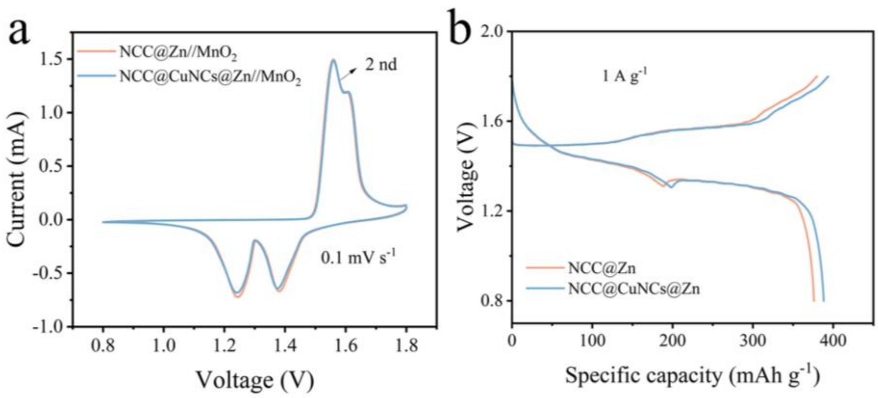

Fig. S24 Comparison of electrochemical performance of Zn//MnO_2 full cells with NCC@Zn and NCC@CuNCs@Zn. (a) CV curves at 0.1 mV s^{-1}. (b) Charge/discharge curves at 1 A g^{-1}.

Table S1 The content of different types of N in NCC

Name	Pyridinic N	Pyrrole N	Graphite N
NCC	11.8%	67.1%	21.1%

Table S2 Comparison of asymmetric cells of this work and reported other substrates

Modified current collector	Electrolyte	Current density (mA cm^{-2})	Capacity (mAh cm^{-2})	Cycle number	CE	Ref.
$Ti_3C_2T_x$ MXene	2.0 M $ZnSO_4$	1.0	1.0	400	94.13%	2
		5.0	1.0	400	-	
CNT	2.0 M $ZnSO_4$	2.0	2.0	30	97.9%	3
LM@CC	2.0 M $ZnSO_4$	1.0	-	500	＞99%	4
AgNPs@CC	1.0 M Zn $(CF_3SO_3)_2$	5.0	2.0	800	99.5%	5
TiOx/Zn-NC	2.0 M $ZnSO_4$	5.0	1.0	1000	98.6%	6
NSH	1.0 M $ZnSO_4$	2.0	1.0	＞200	99%	7
CNF-Zn	2.0 M $ZnSO_4$	2.0	1.0	450	99.5%	8
		5.0	2.0	300	99.8%	
Cu-PAN	2.0 M $ZnSO_4$	2.0	1.0	120	-	9
NCC@CuNCs	2.0 M $ZnSO_4$	1.0	1.0	1000	99.4%	This work

Table S3 Comparison of symmetric cells of this work and reported other substrates

Host	Electrolyte	Current density (mA cm^{-2})	Capacity (mAh cm^{-2})	Cycle life (h)	Ref.
AgNPs@CC	1 M Zn $(CF_3SO_3)_2$	2.0	2.0	800	5
PANI@CC	3.0 M $ZnSO_4$ + 0.1 M $MnSO_4$	0.25	0.05	250	10
		2.0	0.1	88	
CC-CNF	2.0 M $ZnSO_4$	0.25	0.25	400	11
CNT	2.0 M $ZnSO_4$	2.0	2.0	200	3
		5.0	2.5	110	
LM@CC	2.0 M $ZnSO_4$	2.0	1.0	300	4
Cu mesh	1.0 M $ZnSO_4$+0.5 M Na_2SO_4 +1 g L^{-1} PAM	0.2	1.0	350	12
N-VG@CC	2.0 M $ZnSO_4$	0.5	0.5	150	13
		1.0	1.0	65	
$Ti_3C_2T_x$ MXene	2.0 M $ZnSO_4$	1.0	1.0	300	2
3D porous Cu skeleton	2.0 M $ZnSO_4$	0.5	0.5	350	14
TiOx/Zn-NC	2.0 M $ZnSO_4$	1.0	1.0	450	6
Cu mesh@CuO	1.0 M $ZnSO_4$	1.0	1.0	340	15
CNF-Zn@Zn	2.0 M $ZnSO_4$	2.0	1.0	260	8
Cu-PAN	2.0 M $ZnSO_4$	2.0	1.0	270	9
O，N-CC	2.0 M $ZnSO_4$	2.0	2.0	240	16
ACC-600@Cu^{2+}	2.0 M $ZnSO_4$	2.0	2.0	250	17
NCC@CuNCs	2.0 M $ZnSO_4$	1.0	1.0	513	This work
		2.0	2.0	400	This work

References

1. X. Zhang, L. Zhang, X. Jia, W. Song and Y. Liu, Design Strategies for Aqueous Zinc Metal Batteries with High Zinc Utilization: From Metal Anodes to Anode-Free Structures, *Nano-Micro Lett.*, 2024, **16**, 75.
2. X. Li, M. Li, K. Luo, Y. Hou, P. Li, Q. Yang, Z. Huang, G. Liang, Z. Chen, S. Du, Q. Huang and C. Zhi, Lattice Matching and Halogen Regulation for Synergistically Induced Uniform Zinc Electrodeposition by Halogenated Ti_3C_2 MXenes, *ACS Nano*, 2022, **16**, 813-822.
3. Y. X. Zeng, X. Y. Zhang, R. F. Qin, X. Q. Liu, P. P. Fang, D. Z. Zheng, Y. X. Tong and X. H. Lu, Dendrite-Free Zinc Deposition Induced by Multifunctional CNT Frameworks for Stable Flexible Zn-Ion Batteries, *Adv. Mater.*, 2019, **31**, 1903675.
4. X. Jiang, Y. Lam, W. Li, S. Jiang and H. Jia, Self-healing composite anode induced by liquid-metal interlayer for flexible Zn ion storage application, *Compos. Commun.*, 2024, **45**, 101796.
5. T. Chen, Y. Wang, Y. Yang, F. Huang, M. Zhu, B. T. W. Ang and J. M. Xue, Heterometallic Seed-Mediated Zinc Deposition on Inkjet Printed Silver Nanoparticles Toward Foldable and Heat-Resistant Zinc Batteries, *Adv. Funct. Mater.*, 2021, **31**, 2101607.
6. P. X. Sun, Z. Cao, Y. X. Zeng, W. W. Xie, N. W. Li, D. Luan, S. Yang, L. Yu and X. W. D. Lou, Formation of Super-Assembled TiO_x/Zn/N-Doped Carbon Inverse Opal Towards Dendrite-Free Zn Anodes, *Angew. Chem., Int. Ed.*, 2022, **61**, e202115649.
7. Q. Jian, Z. Guo, L. Zhang, M. Wu and T. Zhao, A hierarchical porous tin host for dendrite-free, highly reversible zinc anodes, *Chem. Eng. J.*, 2021, **425**, 130643.
8. J.-H. Wang, L.-F. Chen, W.-X. Dong, K. Zhang, Y.-F. Qu, J.-W. Qian and S.-H. Yu, Three-Dimensional Zinc-Seeded Carbon Nanofiber Architectures as Lightweight and Flexible Hosts for a Highly Reversible Zinc Metal Anode, *ACS Nano*, 2023, **17**, 19087-19097.
9. S. Kumar, H. Yoon, H. Park, G. Park, S. Suh and H.-J. Kim, A dendrite-free anode for stable aqueous rechargeable zinc-ion batteries, *J. Ind. Eng. Chem.*, 2022, **108**, 321-327.
10. Y. Li, Z. X. Tan, Y. S. Liang, Y. Xiao, D. D. Cen, Y. L. Liu and Y. R. Liang, Amine-Functionalized Carbon Cloth Host for Dendrite-Free Zn Metal Anodes, *ACS Appl. Energy Mater.*, 2021, **4**, 4482-4488.
11. Z. Jiang, S. Zhai, L. Shui, Y. Shi, X. Chen, G. Wang and F. Chen, Dendrite-free Zn anode supported with 3D carbon nanofiber skeleton towards stable zinc ion batteries, *J. Colloid Interface Sci.*, 2022, **623**, 1181-1189.
12. Q. Zhang, J. Y. Luan, L. Fu, S. G. Wu, Y. G. Tang, X. B. Ji and H. Y. Wang, The Three-Dimensional Dendrite-Free Zinc Anode on a Copper Mesh with a Zinc-Oriented Polyacrylamide Electrolyte Additive, *Angew. Chem., Int. Ed.*, 2019, **58**, 15841-15847.
13. Q. H. Cao, H. Gao, Y. Gao, J. Yang, C. Li, J. Pu, J. J. Du, J. Y. Yang, D. M. Cai, Z. H. Pan, C. Guan and W. Huang, Regulating Dendrite-Free Zinc Deposition by 3D Zincopilic Nitrogen-Doped Vertical Graphene for High-Performance Flexible Zn-Ion Batteries, *Adv. Funct. Mater.*, 2021, **31**, 2103922.
14. Z. Kang, C. L. Wu, L. B. Dong, W. B. Liu, J. Mou, J. W. Zhang, Z. W. Chang, B. Z. Jiang, G. X. Wang, F. Y. Kang and C. J. Xu, 3D Porous Copper Skeleton Supported Zinc Anode toward High Capacity and Long Cycle Life Zinc Ion Batteries, *ACS Sustainable Chem. Eng.*, 2019, **7**, 3364-3371.
15. Q. Zhang, J. Y. Luan, X. B. Huang, L. Zhu, Y. G. Tang, X. B. Ji and H. Y. Wang, Simultaneously Regulating the Ion Distribution and Electric Field to Achieve Dendrite-Free Zn Anode, *Small*, 2020, **16**, 2000929.
16. M. Zhou, G. Sun and S.-Q. Zang, Uniform zinc deposition on O,N-dual functionalized carbon cloth current collector, *J. Energy Chem.*, 2022, **69**, 76-83.
17. M. Zhou, Z. Wu, R. Wang, G. Sun and S.-Q. Zang, An in situ reduction strategy toward dendrite-free Zn anodes, *Sci. China Mater.*, 2023, **66**, 1757-1766.